ACS NANO

www.acsnano.org

ARTICLE

Chemotherapy-Sensitized *In Situ* Vaccination for Malignant Osteosarcoma Enabled by Bioinspired Calcium Phosphonate Nanoagents

Yangyun Wang, Yanxian Wu, Liubing Li, Chunjie Ma, Shaodian Zhang, Subin Lin, Leshuai W. Zhang, Yong Wang,* and Mingyuan Gao*

Cite This: *ACS Nano* 2023, 17, 6247−6260

Read Online

ACCESS | Metrics & More | Article Recommendations | Supporting Information

ABSTRACT: **How to effectively treat malignant osteosarcoma remains clinically challenging. Programmed delivery of chemotherapeutic agents and immunostimulants may offer a universal strategy for killing osteosarcoma cells while simultaneously eliciting *in situ* antitumor immunity. However, targeted chemoimmunotherapy lacks a reliable delivery system. To address this issue, we herein developed a bioinspired calcium phosphonate nanoagent that was synthesized by chemical reactions between Ca^{2+} and phosphonate residue from zoledronic acid using bovine serum albumin as a scaffold. In addition, methotrexate combination with a phosphorothioate CpG immunomodulator was also loaded for pH-responsive delivery to enable synergistic chemoimmunotherapy of osteosarcoma. The calcium phosphonate nanoagents were found to effectively accumulate in osteosarcoma for nearly 1 week, which is favorable for exerting the vaccination effects *in situ* by maturing dendritic cells and priming $CD8^+$ T cells to suppress the osteosarcoma progression and pulmonary metastasis through controlled release of the three loaded agents in the acidic tumor microenvironment. The current study may thus offer a reliable delivery platform for achieving targeted chemotherapy-induced *in situ* antitumor immunity.**

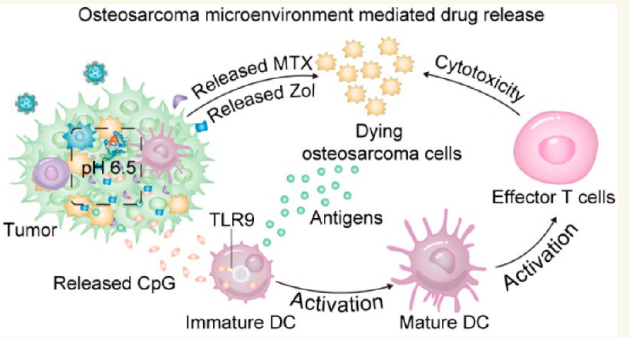

KEYWORDS: *calcium phosphonate nanoagents, bioinspired synthesis, in situ vaccination, chemoimmunotherapy, osteosarcoma*

INTRODUCTION

Malignant osteosarcoma is the most common bone tumor that occurs predominantly in children and adolescents.[1] The current management strategy for osteosarcoma remains surgical resection followed by neoadjuvant chemotherapy. Nevertheless, complete removal of cancer cells in the osteosarcoma microenvironment is difficult, which often results in treatment failure.[2] Although neoadjuvant chemotherapy offers a 5-year survival rate of approximately 60%, it drops to less than 20% when lung metastasis occurs.[2,3] Immunotherapy with a checkpoint blockade has come a long way in fighting malignant tumors, as exemplified by the clinical success of CTLA4 and PD-1/PD-L1 blocking antibodies.[4] The therapeutic efficacy depends largely on the response of effective antigen-specific $CD8^+$ T cells in killing their target tumor cells.[5] However, tumor microenvironment factors including nutrient depletion, hypoxia, and acidosis impair the function of $CD8^+$ T cells, thus the current checkpoint blockade often also suffers from individual differences, poor response rate, and even adverse autoimmune diseases.[6−8]

To extend the duration of response and overcome the adverse side effects, *in situ* vaccination is emerging as an alternative approach for achieving antitumor immune responses through intratumoral injection of oncolytic virus or adjuvants, including stimulators of interferon genes and Toll-like receptor agonists.[9−11] To potentiate systemic antitumor immunity, successful *in situ* vaccines should ideally be able to combine antigens and adjuvants to enhance antigen presentation, subsequently activate the dendritic cells (DCs), and trigger antigen-specific T cell responses.[12] Usually,

Received: September 28, 2022
Accepted: March 21, 2023
Published: March 24, 2023

Scheme 1. Innovative Immunogenic Chemotherapy-Induced *In Situ* Vaccination Strategy for Osteosarcoma through pH-Triggered Release of Zol, CpG, and MTX Loaded by Calcium Phosphonate Nanoagents Formed *via* BSA-Inspired Biomineralization

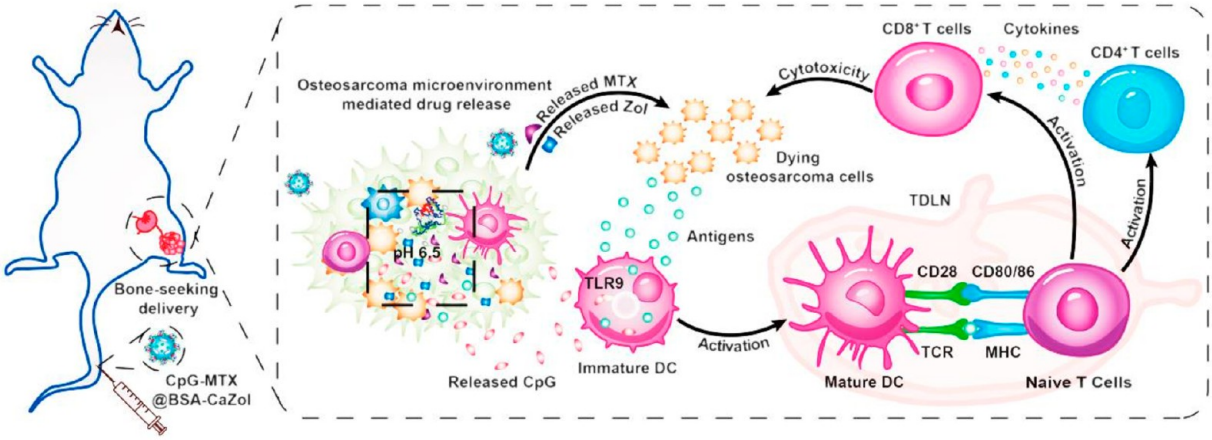

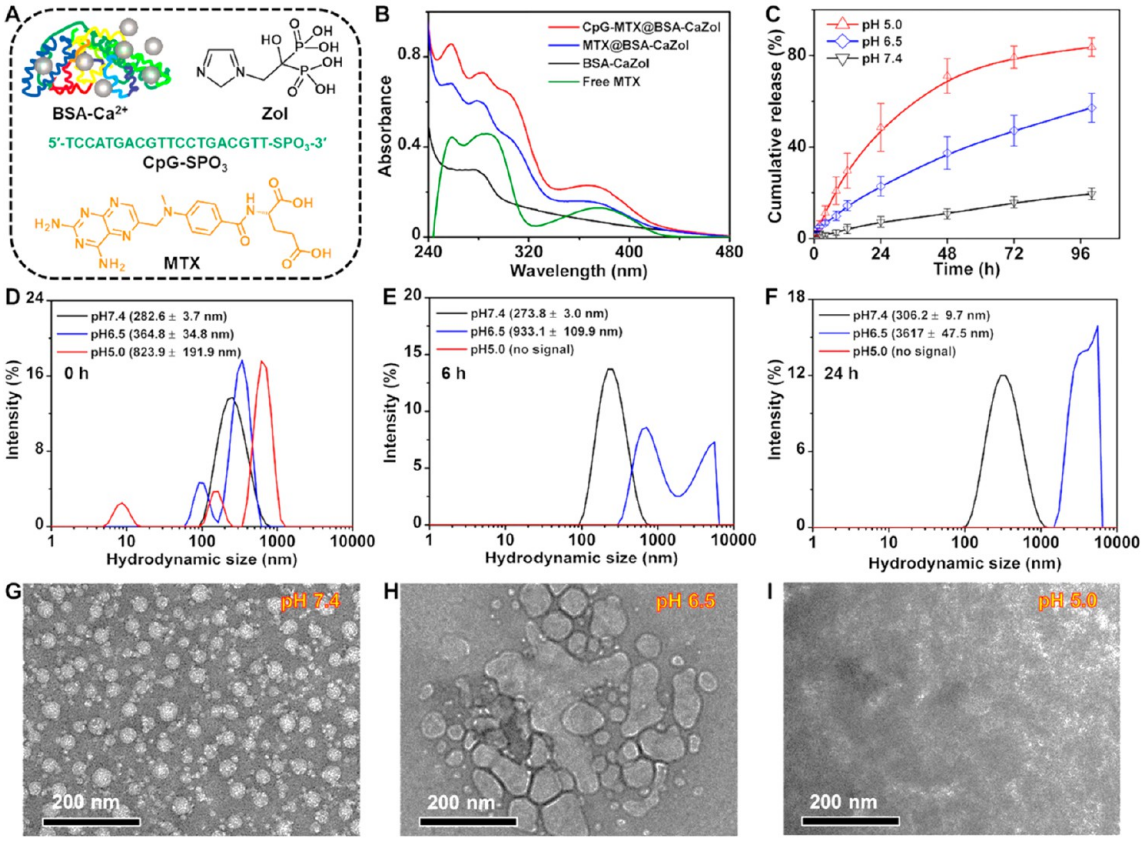

Figure 1. (A) Chemical structures of the major components for forming CpG-MTX@BSA-CaZol and its controls. (B) Absorption spectra of CpG-MTX@BSA-CaZol, MTX@BSA-CaZol, BSA-CaZol, and MTX (302 nm). (C) Cumulative release of MTX from CpG-MTX@BSA-CaZol at different pH. (D−F) Hydrodynamic size profiles of CpG-MTX@BSA-CaZol recorded at different pH upon incubation for 0, 6, and 24 h, respectively. (G−I) TEM images of CpG-MTX@BSA-CaZol recorded after being incubated at different pH for 2 h.

phototherapy, radiotherapy, and chemotherapy are expected to induce the release of tumor-associated antigens (TAA) from immunogenic cell death (ICD),[13−15] and these autologous TAA are expected to overcome the tumor heterogeneity and ineffective delivery of the traditional vaccines.[16] However, owing to the limited penetration depth of phototherapy and radioresistance of radiation therapy, chemotherapy combined with immunotherapy has become a rational choice for the treatment of osteosarcoma.[17,18] In this respect, the use of ICD-inducing chemotherapeutic drugs is expected to offer a promising *in situ* vaccination for killing primary osteosarcoma cells, while simultaneously preventing distant metastasis.[19−21] The conventional chemotherapeutic drugs often suffer from inadequate circulation half-life and limited intratumoral accumulation as well as off-target toxicities.[22−24] To overcome these problems, versatile targeted delivery systems based on

https://doi.org/10.1021/acsnano.2c09685
ACS Nano 2023, 17, 6247−6260

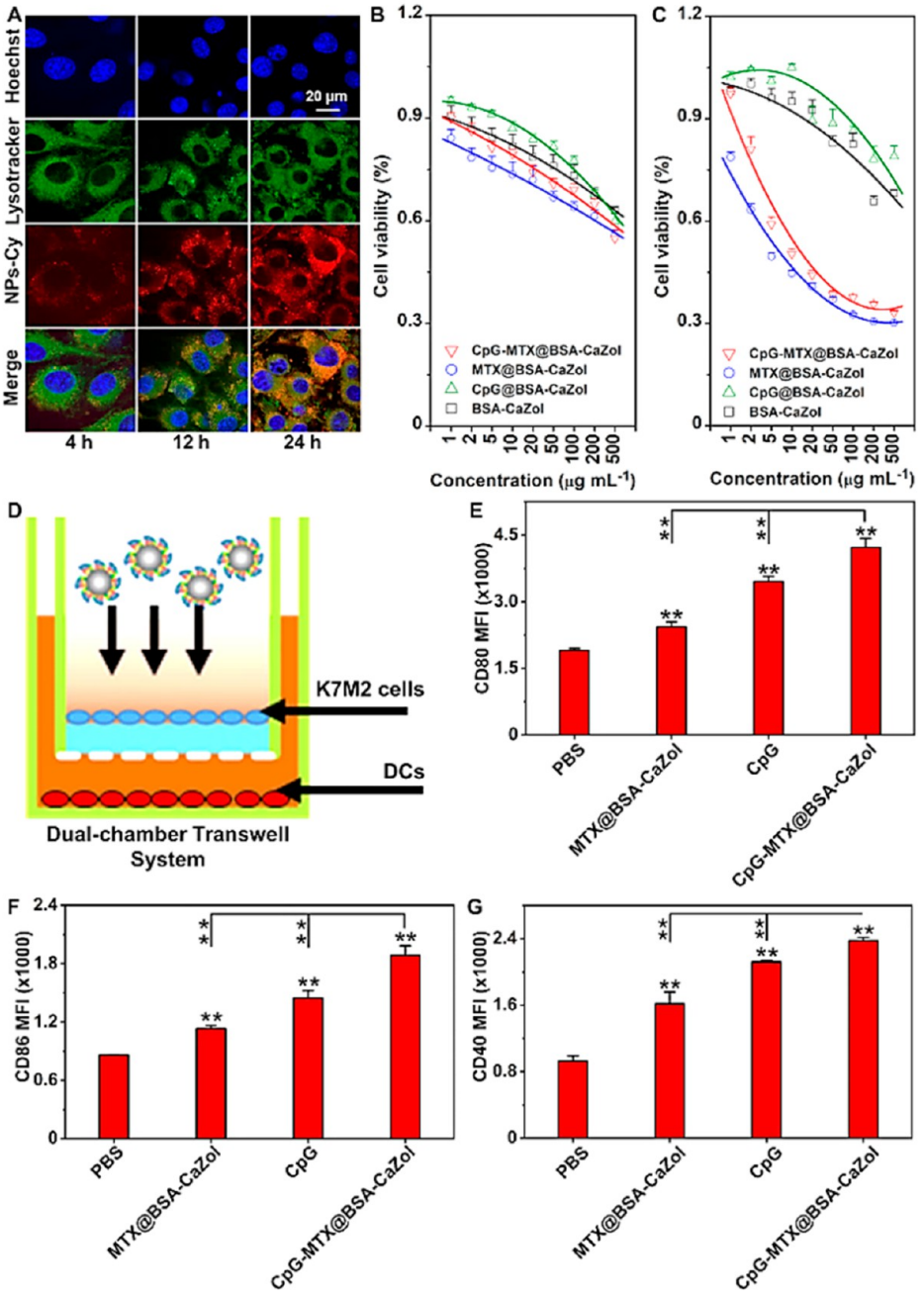

Figure 2. (A) Snapshots of intracellular distribution of Cy-labeled calcium phosphonate nanoagents. (B,C) Cytotoxicity of calcium phosphonate nanoagents to 3T3 cells (B) and K7M2 cells (C), respectively, evaluated by CCK-8 method. (D) *In vitro* chemo-immunotherapeutic effects of CpG-MTX@BSA-CaZol were investigated by coculturing DCs with K7M2 cells in a dual-chamber Transwell for 24 h. (E−G) Expression levels of dendritic cell's maturation markers, i.e., CD80 (E), CD86 (F), and CD40 (G), determined by flow cytometry. All data are expressed by mean ± SD (n = 3). Statistical significance was calculated *via* one-way ANOVA with the Tukey posthoc test (*p < 0.05; **p < 0.01; ***p < 0.001; ****p < 0.0001).

self-organized lipids and biocompatible nanoparticles are being developed.[25,26] Despite the attractive prospects of this strategy, how to achieve an optimal outcome with chemoimmunotherapy remains challenging. In addition, the adjuvants may face difficulty for being efficiently internalized into DCs due to their hydrophobic or anionic nature or enzymatic degradation.[27,28]

Herein, we propose an immunogenic chemotherapy-induced *in situ* vaccination *via* programmed delivery of chemotherapeutic agents and adjuvants, as shown in Scheme 1. It is known that TAA released from chemotherapy-induced ICD can activate DCs, while a short-stranded oligodeoxynucleotide containing an unmethylated cytosine−phosphonate−guanine (CpG) motif can further improve this ability by binding with the Toll-like receptor 9 (TLR9) of DCs, while bisphosphonate zoledronic acid (Zol) has been shown to have selective cytotoxicity to bone metastases to prolong the survival of cancer patients. Inspired by these facts, we designed a pH-sensitive calcium phosphonate nanoagent that was fabricated by using bovine serum albumin (BSA) as a scaffold and Zol as donors of the phosphonate group. In addition, methotrexate

https://doi.org/10.1021/acsnano.2c09685
ACS Nano 2023, 17, 6247−6260

(MTX) was encapsulated for synergistic chemoimmunotherapy of osteosarcoma together with Zol and a CpG immunomodulator. The stability of the resulting nanoagents under physiological conditions and effective release of the payload at the tumor microenvironment pH (6.5−6.9) were studied. In addition, the bone-seeking capacity of the resulting nanoagents, the efficacy for treating osteosarcoma, and particularly the inhibition of pulmonary metastasis were carefully investigated to show the potential of targeted chemotherapy-induced vaccination for sensitizing robust *in situ* antitumor immunity.

RESULTS AND DISCUSSION

Synthesis and Characterization of Calcium Phosphonate Nanoagents. As schematically shown in Figure 1A, the calcium phosphonate (BSA-CaZol) nanoparticles were prepared through BSA-mediated biomineralization upon chemical reactions between Ca^{2+} and zoledronic acid. The nanoparticles formed in the presence of MTX and full-chain phosphorylated CpG were denoted as CpG-MTX@BSA-CaZol, while those prepared in the presence of either cytotoxic MTX or CpG were denoted as MTX@BSA-CaZol and CpG@BSA-CaZol, respectively. The absorption spectroscopy results shown in Figure 1B indicate that the absorbance peak of MTX was 302 nm. MTX molecules are successfully loaded into the nanoagents, and the loading efficiency of MTX is approximately 7.4% according to the absorption spectroscopy results in Figure 1B and Figure S1. In a similar way, the loading efficiency of CpG was determined to be around 0.05% according to the absorption spectroscopy results (Figure S2). The zeta potential of CpG-MTX@BSA-CaZol was about −20 mV, as shown in Figure S3. To verify the protective effect of nanoparticles on CpG, free CpG and CpG-MTX@BSA-CaZol were subjected to DNase treatment and then analyzed by agarose gel electrophoresis. The results in Figure S4 indicated that CpG was effectively degraded by DNase, while CpG-MTX@BSA-CaZol presented much weaker degradation.

Owing to the intrinsic solubility property, calcium phosphonate was used in the literature as a pH-responsive carrier for delivering drugs to tumorous sites. Therefore, it is reasonable to expect the calcium phosphonate nanoagents should also exhibit a similar pH-dependent response. The results shown in Figure 1C verify this hypothesis and further demonstrate that the cumulative release of MTX by CpG-MTX@BSA-CaZol reaches 85.9% at pH 5.0 over a 5 day incubation, while it drops to 61.5% at pH 6.5 and further to 23.1% at pH 7.4. Under normal physiological conditions (pH 7.4), the hydrodynamic size of CpG-MTX@BSA-CaZol is around ∼282.6 nm. As shown in Figure 1D−F, lowering the environmental pH will immediately increase the hydrodynamic size of the nanoagents, probably owing to the protonation of BSA whose isoelectric point is around 4.5−4.8. The nanoagents grow bigger and bigger at pH 6.5 as time goes on, while they gradually vanish when pH was decreased to ∼5.0, owing to the degradation of the calcium phosphonate. These morphological variations were also observed with transmission electron microscopy (TEM). As shown in Figure 1G−I, the initial CpG-MTX@BSA-CaZol composite agents formed at neutral pH are quasi-spherical particles of approximately 30 nm in diameter. These particles form much bigger aggregates at pH 6.5 and eventually get dissolved when the pH value is decreased to 5.0. These pH-dependent behaviors make the calcium phosphonate nanoagents very suitable for pH-triggered release of MTX, apart from Zol and CpG, into the tumor microenvironment.

***In Vitro* Cellular Uptake, Cytotoxicity, and DC Activation.** In order to show the performance of CpG-MTX@BSA-CaZol in delivering MTX, the nanoagent was labeled with a near-infrared fluorescent dye cypate (Cy) for tracking the cellular uptake through fluorescence microscopy. Specifically, the Cy-labeled CpG@BSA-CaZol was incubated with K7M2 osteosarcoma cells for 4, 12, and 24 h. According to confocal microscope observation (Figure 2A), the nanoagents are gradually internalized into cells and finally localized in lysosomes. The cytotoxicity of the CpG-MTX@BSA-CaZol therapeutic nanoagents to normal cells (3T3) and osteosarcoma cells (K7M2) was evaluated. As shown in Figure S5A, CpG was not toxic to 3T3 and K7M2 cells. The results in Figure 2B,C reveal that the MTX-loaded nanoagents exhibit cytotoxicity stronger than that of CpG@BSA-CaZol and BSA-CaZol, probably owing to the synergistic effects of MTX and Zol (Figure S5B), especially for the K7M2 groups. The cell viabilities decreased to 30−40% at the maximum concentration of the MTX-loaded nanoagents, i.e., 500 μg mL^{-1}, suggesting that it is effective to combine MTX with Zol for osteosarcoma treatment.

The effective release of MTX and Zol is critical for inducing ICD to expose TAA from osteosarcoma cells and then together with the released CpG to constitute an *in situ* vaccine. To verify the chemo-immunotherapeutic effects *in vitro*, CpG-MTX@BSA-CaZol was cocultured with K7M2 cells in the upper chamber of a dual-chamber Transwell with DCs being placed in the lower chamber for 24 h, as shown in Figure 2D. The two chambers were separated by a 0.4 μm microporous membrane to allow for the exchange of molecules rather than cells across the membrane. Once MTX is released on the tumor cell side, it will induce cell apoptosis to release antigen that is expected to enter the DC cell side together with the released CpG adjuvant to activate DCs. To show the DC activation effects, the expression levels of DC maturation markers, including CD80, CD86, and CD40, were analyzed by flow cytometry, and MTX@BSA-CaZol, CpG@BSA-CaZol, BSA-CaZol, CpG, MTX, and Zol were used as controls. As shown in Figure 2E−G and Figure S6, the DCs coincubated with CpG-MTX@BSA-CaZol and K7M2 cells present the highest activation levels of the corresponding markers. Compared with nontreated controls, the expression levels of all three phenotypic markers increase by 2−3 factors after 24 h of coincubation. To investigate the effect of CpG@BSA-CaZol and CpG-MTX@BSA-CaZol on DC maturation, the CD80 and CD86 expression of DCs was analyzed by flow cytometry. As shown in Figure S7, CpG@BSA-CaZol and CpG-MTX@BSA-CaZol alone could promote DC maturation because of the TLR9 agonist CpG. Besides, to further verify the DC maturation induced by ICD, the experiment of collecting supernatant of nanoagent-treated K7M2 cells and apply to DCs to monitor maturation has been assessed. The DCs coincubated with the supernatant of CpG-MTX@BSA-CaZol-treated K7M2 cells present the highest activation levels of CD80 and CD86 (Figure S8). All of these results suggest that the current nanoagents can effectively activate and mature DCs *in vitro*.

Chemotherapy-Induced *In Situ* Vaccination. It is known that chemotherapy can induce ICD to release TAA from the dying tumor cells.[29] Then the chemotherapeutic agent-induced ICD is expected to offer a convenient and

https://doi.org/10.1021/acsnano.2c09685
ACS Nano 2023, 17, 6247−6260

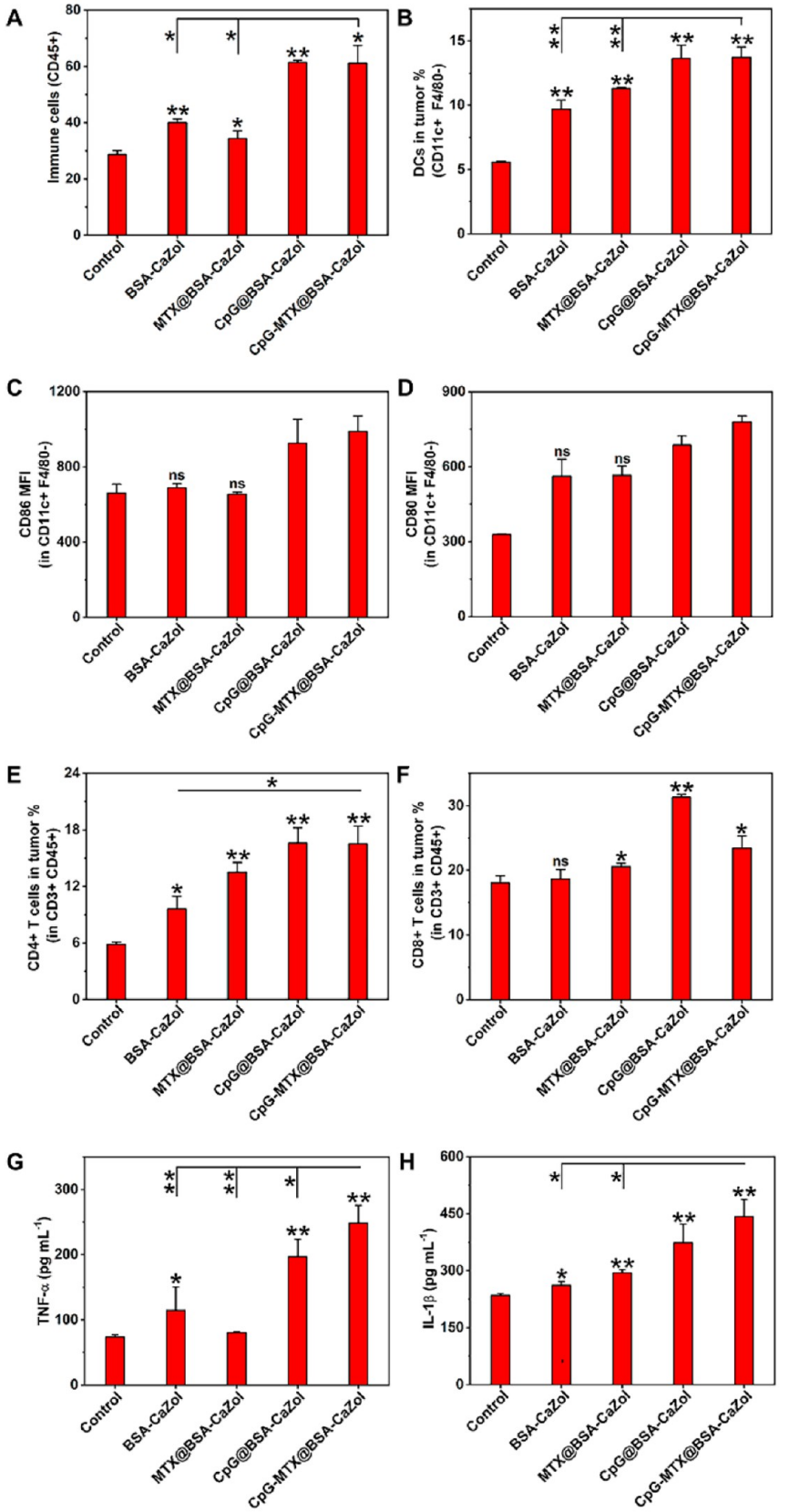

Figure 3. Immune responses of K7M2 tumor-bearing mice intravenously injected with CpG-MTX@BSA-CaZol and its controls, characterized by levels of immune cells (A), DCs (B), CD86 (C), CD80 (D), $CD4^+$ (E), $CD8^+$ T (F) cells in tumors, and levels of TNF-α (G) and IL-1β (H) in serum, on day 3 post-treatment. All data are expressed by mean ± SD (n = 3). Statistical significance was calculated *via* one-way ANOVA with the Tukey posthoc test (*p < 0.05; **p < 0.01; ***p < 0.001; ****p < 0.0001).

https://doi.org/10.1021/acsnano.2c09685
ACS Nano 2023, 17, 6247−6260

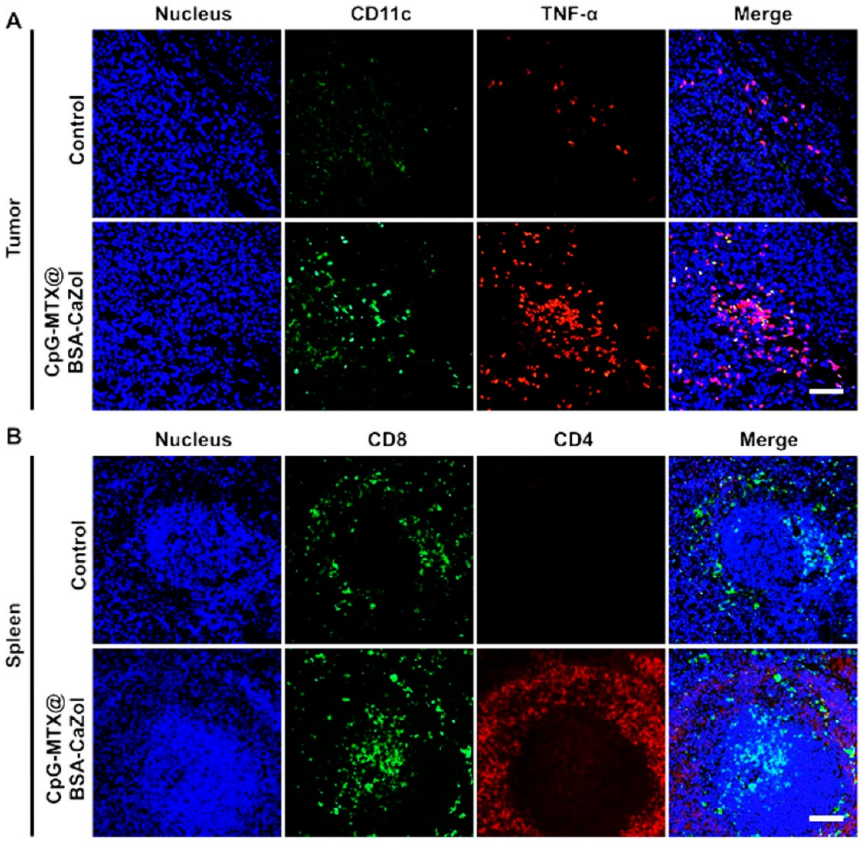

Figure 4. Pathological immunofluorescence analysis of K7M2 tumors and spleens of mice intravenously receiving CpG-MTX@BSA-CaZol performed on day 3 post-treatment to show the expression of $CD11c^+$ DCs and TNF-α in tumors (A), and infiltration of $CD8^+$ and $CD4^+$ T cells into spleen (B) (error bar = 100 μm).

universal antitumor strategy by eliciting broad T cell responses. To verify this hypothesis, K7M2 cells were injected into the left tibia of mice to establish an osteosarcoma mouse model,[30−32] and then DC activation and T cell responses to the calcium phosphonate nanoagents *in vivo* were evaluated. The tumors were collected 3 days postinjection of the nanoagents for flow cytometry analysis. To evaluate the immunogenic cell death induced by CpG-MTX@BSA-CaZol, calreticulin (CRT) and high mobility group box 1 (HMGB-1) were detected. As shown in Figure S9A,B, CRT and HMGB-1 were the highest in CpG-MTX@BSA-CaZol, indicating that CpG-MTX@BSA-CaZol possesses the strongest ability to induce ICD. According to results given in Figure 3A, as compared with nontreated controls, the immune cells in the tumor of mice treated with CpG@BSA-CaZol and CpG-MTX@BSA-CaZol were increased by factors of 1−1.5. DCs in the tumor-associated lymphocytes shown in Figure 3B indicate that the highest proportion come from CpG@BSA-CaZol- and CpG-MTX@BSA-CaZol-treated mice, and DC maturation was naturally stimulated in these two groups (Figure 3C,D). In addition, the mature DCs in the tumor-draining lymph nodes (TDLN) of mice treated with CpG-MTX@BSA-CaZol were increased in comparison with those of the control and MTX +Zol, as shown in Figure S10. Moreover, according to the results in Figure 3E,F and Figure S11, helper $CD4^+$ T cells and cytotoxic $CD8^+$ T cells also gain significant increments in the groups involving CpG, in contrast to the groups with no CpG present, i.e., BSA-CaZol and MTX@BSA-CaZol. Moreover, $CD8^+$ and $CD4^+$ T cells are found to infiltrate into tumors after CpG-MTX@BSA-CaZol treatment, as analyzed by immunofluorescence (Figure S12). In addition, the levels of cytokines in the serum of CpG-MTX@BSA-CaZol-treated mice are also increased by factors of 3.3 (TNF-α) and 1.9 (IL-1β) in comparison with those of the control group, which in return promotes the proliferation of cytotoxic $CD8^+$ T cells. All of the above results indicate that the cytotoxic $CD8^+$ T cells can effectively be primed by CpG-loaded calcium phosphonate nanoagents, which also validates the rationality of *in situ* vaccination for inhibiting the tumor growth.

To further provide direct proof on *in situ* vaccination, the tumor and spleen were extracted and then subjected to pathological immunofluorescence analysis. As shown in Figure 4A, the signals of $CD11c^+$ DCs match well those of TNF-α in tumors treated with CpG-MTX@BSA-CaZol. Immunofluorescence results shown in Figure 4B indicate that both $CD8^+$ and $CD4^+$ T cells can infiltrate into the spleen of mice treated by CpG-MTX@BSA-CaZol, indicating that CpG-MTX@BSA-CaZol can active the systematic and tumor immune response. These immune activation effects lay an essential corner stone for antitumor *in situ* vaccination.[33]

Antiosteosarcoma Effects *In Vivo*. According to the current design, the calcium phosphonate nanoagents should have exhibited bone targeting ability and thus improved retention in osteoblastic lesions.[34] To verify the bone-seeking performance of calcium phosphonate nanoagents *in vivo*, Cy-labeled CpG-MTX@BSA-CaZol and BSA-CaZol were intravenously injected into mice bearing osteosarcoma for fluorescence imaging *in vivo*. As shown in Figure 5A, both

https://doi.org/10.1021/acsnano.2c09685
ACS Nano 2023, 17, 6247−6260

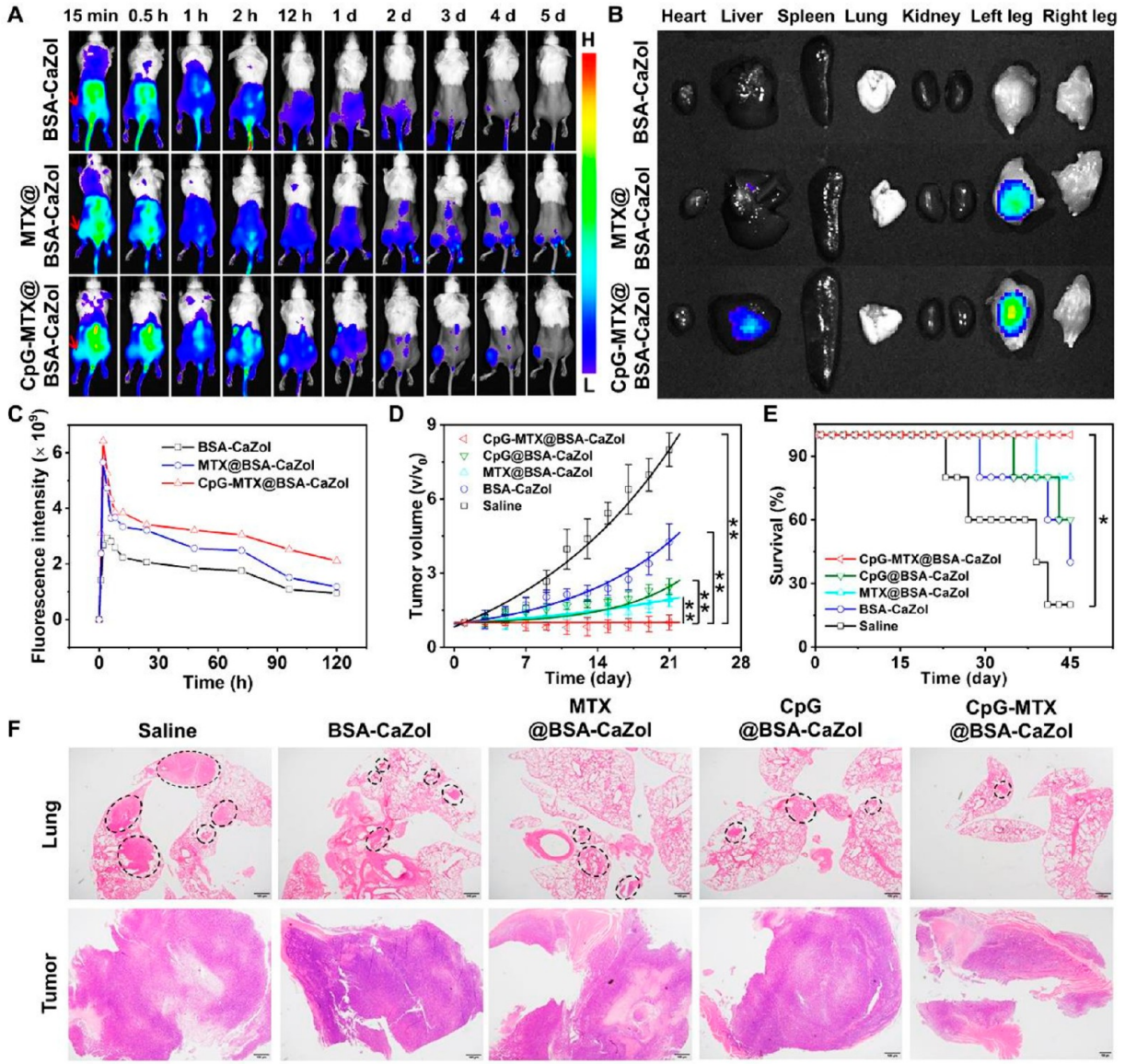

Figure 5. (A) Fluorescence snapshots of osteosarcoma-bearing mice intravenously injected with Cy-labeled calcium phosphonate nanoagents with the tumor sites highlighted with red arrows. (B) *Ex vivo* imaging of different organs, left leg (containing tumor), and right leg at day 5 after the first injection. (C) Tumor fluorescence semiquantitative statistics chart. (D) Tumor growth profiles. (E) Survival rate of osteosarcoma-bearing mice. All data are represented as mean ± SD (*$p < 0.05$; **$p < 0.01$; ***$p < 0.001$; ****$p < 0.0001$). (F) Pathology analysis of lung and tumor of osteosarcoma-bearing mice intravenously injected with calcium phosphonate nanoagents. Lung metastasis sites are highlighted by the dotted circle.

calcium phosphonate nanoagents are distributed in the whole body of mice after intravenous injection. Close observations reveal that CpG-MTX@BSA-CaZol and MTX@BSA-CaZol generate stronger signals than BSA-CaZol in the left leg, where tumors were inoculated, in contrast to the right leg, particularly when the signals from most parts of the body vanish 3 days after delivery of the nanoagents. It should be mentioned that the CpG-MTX@BSA-CaZol agents remain visible even on day 5 postinjection. Moreover, the signals of BSA-CaZol fade faster than those of CpG-MTX@BSA-CaZol, probably because the latter possesses higher stability owing to the involvement of CpG. The *ex vivo* imaging of different organs containing left and right legs at 5 days showed that nanoagents were mainly metabolized from the liver, and nanoagents can accumulate in the tumors for a long time, especially CpG-MTX@BSA-CaZol (Figure 5B). Besides, through fluorescence spectroscopy, it was confirmed that the fluorescence intensity of CpG-MTX@BSA-CaZol was higher than that of BSA-CaZol at each time point (Figure 5C). Moreover, the fluorescence quantitative chart of tumors and some main organs shown in Figure S13 confirmed that nanoagents could be rapidly metabolized and cleared from the body, and high tumor enrichment was shown in CpG-MTX@BSA-CaZol and MTX@BSA-CaZol groups. To investigate the hepatic and renal toxicity of nanoagents, serum AST, ALT, ALP, urea, CREA, and GGT were tested. As shown in Figure S14, there was no significant difference between CpG-MTX@BSA-CaZol and the saline group. All of these results reveal that the excellent bone affinity of CpG-MTX@BSA-CaZol nanoagents can give rise to ultralong retention of the nanoagents, which is beneficial for subsequently activating the

https://doi.org/10.1021/acsnano.2c09685
ACS Nano 2023, 17, 6247−6260

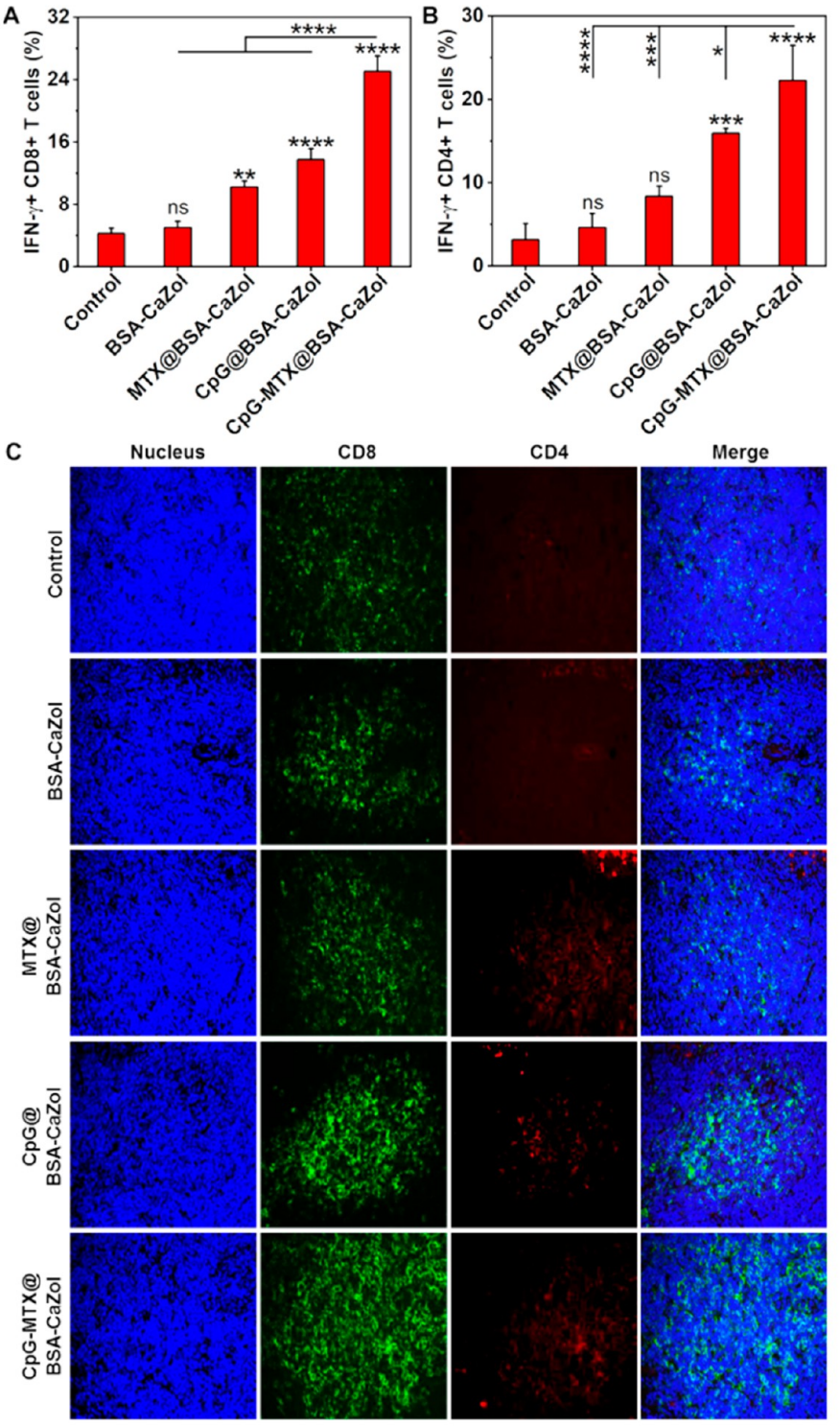

Figure 6. Specific responses of T cells in the tumor microenvironment of osteosarcoma-bearing mice, intravenously injected with various calcium phosphonate nanoagents, were investigated on day 21 post-treatment. (A,B) Flow cytometry analysis of IFN-γ^+ CD8$^+$ and IFN-γ^+ CD4$^+$ T cells in tumors. All data are represented as mean ± SD. Statistical significance was calculated *via* one-way ANOVA with the Tukey posthoc test (*p < 0.05; **p < 0.01; ***p < 0.001; ****p < 0.0001. (C) Infiltration levels of CD8$^+$ and CD4$^+$ T cell in tumors.

immune system to achieve chemotherapy-sensitized antitumor vaccination *in situ*.

In the current design, the bone-targeted Zol relieves malignant osteoblastic progression, MTX kills tumor cells, and the adjuvant CpG enhances the immunogenic death response.[35] To verify CpG-MTX@BSA-CaZol can in this way combine the chemotherapy with *in situ* vaccination, the antitumor effects were carefully investigated by monitoring the tumor growth and survival rates of model mice. As shown in Figure 5D,E and Figure S15A,B, CpG-MTX@BSA-CaZol exhibits the greatest synergistic effects in suppressing the tumor progression and maximizing the overall survival rate of

https://doi.org/10.1021/acsnano.2c09685
ACS Nano 2023, 17, 6247−6260

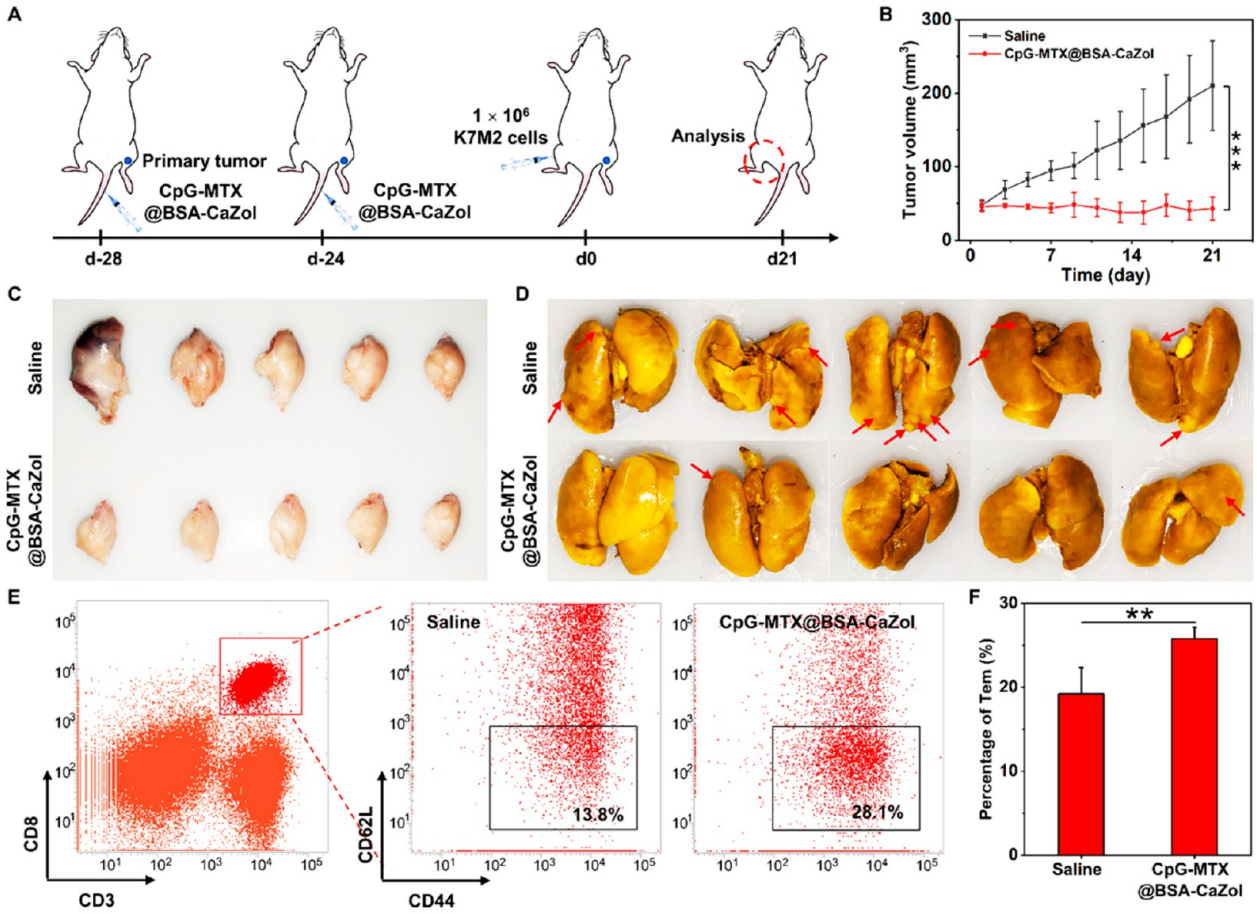

Figure 7. Osteosarcoma rechallenge for verifying the immune memory effect induced by CpG-MTX@BSA-CaZol. (A) Experimental scheme for the rechallenge tests. Primary tumor on the left leg was treated with CpG-MTX@BSA-CaZol (5 mg mL^{-1}, i.v.) on day −28. 1 × 10^6 K7M2 cells were injected into the right leg on day 0 to construct the secondary tumors, and the naïve mice were used as the control (n = 5). (B) Rechallenge osteosarcoma growth curves of naïve and CpG-MTX@BSA-CaZol-treated mice. (C) Osteosarcoma and (D) lung images obtained on day 21 (arrows indicate the pulmonary metastatic nodules). (E,F) Proportions of effector memory T cells (Tem) in the spleen analyzed by flow cytometry (gated on CD3$^+$CD8$^+$ T cells) on day 21 right before rechallenging mice with secondary osteosarcomas.

mice, in comparison with control nanoagents, *e.g.*, CpG@BSA-CaZol, MTX@BSA-CaZol, BSA-CaZol, and MTX+Zol. According to morphological and pathological variations in lungs, as shown in Figure S16 and Figure 5F, CpG-MTX@BSA-CaZol can most effectively alleviate lung metastases of osteosarcoma. The mice from the control groups not only show definite lung metastasis but also indicate the characteristics of solid tumors. The above results indicate that CpG-MTX@BSA-CaZol nanoagents can induce *in situ* antitumor immunity with tumor-associated antigens from apoptotic osteoblasts and CpG released from calcium phosphonate nanoagents, which gives rise to markedly potentiate synergistic therapeutic efficacy and leads to elimination of osteosarcoma and pulmonary metastasis.

To reveal the immune responses induced by *in situ* vaccination, infiltration of specific DCs and T cells in the tumor microenvironment was investigated. On day 21 post-treatment, the mice were sacrificed post-anesthesia. The tumors and spleens were collected and made into suspensions for flow cytometry and ELISA measurements (Figure S17). Moreover, splenomegaly studies on draining LNs showed that a local immune response was induced by CpG-loaded calcium phosphonate nanoagents in comparison to the mother calcium phosphonate nanoagents (Figure S18). The results shown in Figure 6A and Figure S19 further reveal that the percentage of cytotoxic CD8$^+$ T cells in the tumor of mice treated with CpG@BSA-CaZol and CpG-MTX@BSA-CaZol, respectively, is increased by factors of 3−6 in comparison with those of the corresponding nontreated controls. Similarly, the content of CD4$^+$ T cells is increased by a factor of 5−7 in comparison with that of the untreated control, as shown in Figure 6B and Figure S19. All of these results indicate that the cytotoxic CD8$^+$ and CD4$^+$ T cells can effectively be primed by CpG-loaded calcium phosphonate nanoagents in the tumor microenvironment.

To further visualize the infiltration of CD11c$^+$ DCs and CD8$^+$ T cells and the expression of TNF-α in the tumor and spleen, pathological immunofluorescence studies were carried out. As shown in Figures S20 and S21, the locations of CD11c$^+$ DC signals match well with those for TNF-α in both tumors and spleens of mice treated by CpG-MTX@BSA-CaZol. Moreover, as showcased in Figure 6C, the infiltration of CD8$^+$ T cells into tumors is improved for mice treated with CpG@BSA-CaZol and CpG-MTX@BSA-CaZol nanoagents. However, the infiltration of CD4$^+$ T cells is not obvious, indicating that CD8$^+$ T cell infiltration is largely responsible for the antitumor immunity. Further blood biochemistry and pathological analysis revealed that the bone-seeking capacity of

https://doi.org/10.1021/acsnano.2c09685
ACS Nano 2023, 17, 6247−6260

the CpG-MTX@BSA-CaZol nanoagents greatly enhanced the potency of CpG while simultaneously lowering systemic side effects of in situ vaccination for short-term (Figure S22) and long-term toxicity (Figures S23 and S24). To further verify the important role of CD8 in antitumor immunity of CpG-MTX@BSA-CaZol, CD8 depletion experiments were carried out. As shown in Figure S25A, anti-mouse CD8 antibody was intraperitoneally administered continually on days −2, −1, and 0 and then injected with CpG-MTX@BSA-CaZol intravenously on day 1. After depletion of $CD8^+$ T cells, CpG-MTX@BSA-CaZol did not inhibit tumor growth due to the limited CD8 T cell infiltration (Figure S25B), indicating the crucial role of CD8 in antitumor immunity.

To verify the universality of CpG-MTX@BSA-CaZol for antibone tumor treatment, the therapeutic efficacy of CpG-MTX@BSA-CaZol for treating bone metastasis of breast cancer was evaluated. As shown in Figure S26A, bioluminescence signals of 4T1-Luc cells were used to monitor the tumor growth. Mice treated with CpG-MTX@BSA-CaZol showed significant tumor inhibition effects in comparison with that of the saline group (Figure S26B). Similarly, CpG-MTX@BSA-CaZol could prolong the survival rate of tumor-bearing mice (Figure S26C). As shown in Figure S26D, lung metastases nearly occurred in the saline group but not in the CpG-MTX@BSA-CaZol-treated group. These results demonstrated that CpG-MTX@BSA-CaZol possesses antitumor effects not only on osteosarcoma but also on bone metastases of other cancers.

Osteosarcoma Rechallenge for Verifying the Immune Memory Effect. To verify the systemic immune memory response that is crucial for preventing osteosarcoma from metastasis and relapse. Osteosarcoma rechallenge experiments were performed on the mice completely recovered from primary tumor challenge upon treatment with CpG-MTX@BSA-CaZol to show the antiosteosarcoma memory effect (Figure 7A). Osteosarcoma volume analysis supports a significant inhibition of secondary osteosarcoma growth in the mice vaccinated with CpG-MTX@BSA-CaZol, in contrast to age-matched naïve mice (Figure 7B,C and Figure S27). Moreover, fewer lung nodules were shown in the CpG-MTX@BSA-CaZol group than in the saline group (Figure 7D). All of these results demonstrate that CpG-MTX@BSA-CaZol can induce a strong immune protective effect. To disclose the mechanism of antitumor immune memory, effector memory T cells (Tem) in the spleen were harvested and analyzed on day 21 post-treatment. Notably, the percentage of Tem cells ($CD3^+CD8^+$ $CD44^+CD62L^-$) after CpG-MTX@BSA-CaZol treatment was much higher than that in naïve mice (Figure 7E,F). To further confirm the immune memory effect, the splenocytes from CpG-MTX@BSA-CaZol-treated mice were cocultured with K7M2 cells for 24 h, and then the intracellular IFN-γ and Granzyme B production by $CD8^+$ T cells were detected by cytometry. The $CD8^+$ T cells from CpG-MTX@BSA-CaZol-treated mice promoted more IFN-γ and Granzyme B production than from naïve mice after being restimulated by K7M2 cells (Figure S28). Thus, it can be concluded that CpG-MTX@BSA-CaZol nanoagents can induce a strong immune memory to effectively inhibit the recurrence of cancer through Tem cells.

CONCLUSIONS

In summary, an *in situ* vaccination sensitized by chemotherapy has been proposed and demonstrated to be effective for antiosteosarcoma, with bioinspired calcium phosphonate nanoagents composed of Zol, MTX, and CpG, apart from BSA as a scaffold. Systematic studies have shown that the properties of calcium phosphonate enable pH-responsive delivery of the chemotherapeutic agents and immunostimulants to osteosarcoma, while Zol provides the nanoagents with specific bone-binding capacity, apart from inducing the release of tumor-associated antigens from immunogenic cell death together with MTX. The *in vivo* experiments demonstrate that the current nanoagents can effectively eliminate osteosarcoma and pulmonary metastasis, which verifies the *in situ* vaccination concept enabled by chemotherapy for the treatment of bone tumors.

EXPERIMENTAL SECTION

Materials and Reagents. Bovine serum albumin, calcium chloride anhydrous, and 25% ammonium hydroxide were purchased from Sinopharm Group Chemical Reagent Co., Ltd. Zoledronic acid was purchased from TCI (Shanghai) Development Co., Ltd. Methotrexate was purchased from Sigma-Aldrich. A 20 bp DNA ladder was purchased from TaKaRa (China). Anti-mouse antibodies against CD40, CD80, CD86, and CD11c were purchased from BD Pharmingen (San Diego, CA, USA), and MHCII was purchased from Sigma-Aldrich. AlexaFluor488-conjugated calreticulin was purchased from Abcam. eFluor@506-conjugated CD45, APC-conjugated F4/80, APC-conjugated CD3, FITC-conjugated CD4, PerCP-Cy5.5-conjugated CD8, PE-conjugated CD44, and BV421-conjugated CD62L were obtained from Biolegend (San Diego, CA, USA). All other chemicals were obtained from Aladdin (Shanghai, China).

Synthesis and Characterization. BSA-CaZol were prepared as follows. An aqueous solution of 5 mL containing BSA (30 mg mL^{-1}) and $CaCl_2$ (0.15 M) was prepared. In parellel, another aqueous solution of 5 mL containing both zoledronic acid (0.02 M) and ammonium hydroxide (2.5%) was also prepared. Then the two solutions were mixed at 37 °C at pH 10. The mixture obtained after a 16 h incubation was subjected to dialysis using a membrane with a cutoff molecular weight of 7000 Da for 24 h. The MTX-loaded nanoagents were prepared the same way as mentioned above except that 5 mg of MTX was predissolved in zoledronic acid solution. Regarding the CpG-loaded nanoagents, 280 μL of CpG solution (100 mM) was introduced into the solution containing BSA and Ca^{2+}.

Transmission electron microscopy (Tecnai G2 spirit BioTwin, FEI) was used to characterize the morphology of all nanoagents. Measurements of hydrodynamic size and charge were conducted using dynamic light scattering (Zetasizer ZS90, Malvern). The absorbance spectra was measured with a UV−vis−NIR spectrophotometer (Lambda 35, PerkinElmer). The loading efficiency of CpG was analyzed by absorption spectroscopy results of Cy5.5-labeled CpG (Sangon Biotech, China).

pH-Responsive Release of MTX. The release of MTX from CpG-MTX@BSA-CaZol nanoparticles was investigated *in vitro* after being dialyzed against buffer solutions of different pH. Briefly, 1 mL nanoparticles (5 mg mL^{-1}) in triplicate were added to dialysis bags (3500 Da). The three dialysis bags were immersed in MES buffer (5 mL) at one of the following pH: 5.0, 6.5, 7.4. The dialysis was carried out at 37 °C under shaking at 100 rpm. At selected time points, 500 μL of buffer was withdrawn for UV−vis spectroscopy analysis at 302 nm, and the same amount of fresh MES buffer was added. For all samples, the drug releasing behavior was continuously monitored for 3 days.

Enzymatic Degradation Experiments. In brief, CpG-MTX@BSA-CaZol and CpG were incubated with DNase I (5 U μL^{-1}) at 37 °C for 20 min. The reaction mixture was analyzed by 3% agarose gel electrophoresis. CpG-MTX@BSA-CaZol and CpG were used as controls.

Cells and Animals. NIH-3T3 and K7M2 cells (murine osteosarcoma cells) were obtained from Cell Institute of Chinese Academy of Sciences (Shanghai, China) and cultured in DMEM

https://doi.org/10.1021/acsnano.2c09685
ACS Nano 2023, 17, 6247−6260

containing 10% FBS and 1% penicillin−streptomycin solution under standard conditions (37 °C and 5% CO_2).

All animal experiments were approved by Animal Ethics Committee of Soochow University (Suzhou, China). The national guidelines for laboratory animal care and use were followed in all animal experiments (certificate no. 20020008, grade II). The male C57BL/6 mice (4−6 weeks) and female BALB/c mice (4−6 weeks) were obtained from Shanghai SLAC Laboratory Animal.

The K7M2 orthotopic osteosarcoma model was established using 6-week-old female BALB/c mice according to the protocols provided in the literature.[31] Briefly, the suspension of K7M2 cells (2×10^6 cells per 50 μL in 1× PBS) was injected into the intramedullary cavity of the left tibia. After transplantation, the animals were well fed under standard conditions for 15 days before the following experiments. The method used for measuring tumor volume of osteosarcoma was borrowed from the literature.[36,37] In brief, a vernier caliper was used to measure the anteroposterior and left−right diameters of the tibia at the tumor site in mice, and then the tumor size was calculated according to the formula $V = L \times W^2/2$.

Bone-marrow-derived dendritic cells were obtained from C57BL/6 mice based on a previously described protocol.[38] DCs were cultured in RPMI 1640 containing 10% FBS and 1% penicillin−streptomycin solution under standard conditions (37 °C and 5% CO_2).

Cellular Uptake and Cytotoxicity of Nanoagents. Standard conditions (37 °C and 5% CO_2) were used to culture K7M2 cells. To evaluate the cellular uptake and intracellular trafficking of CpG@BSA-CaZol, K7M2 cells (5×10^5 cells) were seeded in 35 mm cultured dishes and incubated with CpG@BSA-CaZol (100 μg mL^{-1}) for 2, 4, 12, and 24 h. At selected time points, the cells were washed with PBS twice and reincubated again with fresh DMEM containing LysoTracker green (100 nM) for 1 h. After that, the cells were stained for 30 min with Hoechst 33342 (0.5 μg mL^{-1}). Before being imaged with a confocal fluorescence microscope, the cells were fixed with 4% paraformaldehyde for 15 min and then washed with PBS twice.

K7M2 cells were seeded into 96-well plates at the density of 10,000 cells per well and allowed to attach for 24 h. Then the cells were exposed to various concentrations of BSA-CaZol, MTX@BSA-CaZol, CpG@BSA-CaZol, and CpG-MTX@BSA-CaZol for another 24 h. After incubation, cell viability was measured by with a CCK8 assay (Dojindo, Japan). The viability of NIH-3T3 cells was evaluated using same method.

DC Maturation *In Vitro*. Murine bone marrow cells were seeded in six-well plates and incubated for 1 week, and the medium was refreshed every 2 days. Finally, 1×10^5 cells per well were seeded in 24-well plates and cultured with the control, free CpG, free MTX, free Zol, MTX@BSA-CaZol, and CpG-MTX@BSA-CaZol for 24 h. The cells were collected through centrifugation at 800 rpm for 5 min and washed. After decanting the supernatant, one portion of DCs was stained with anti-mouse antibodies against CD40-PE and CD11c-PerCP/Cy5.5 and another with CD80-PE, CD86-FITC, and CD11c-PerCP/Cy5.5. The maturation of DCs was evaluated on a FACS Calibur flow cytometer (BD Bioscience).

To evaluate indirect DC maturation, K7M2 cells (1×10^5 cells/well) were cultured with the control, free CpG, free MTX, free Zol, and CpG-MTX@BSA-CaZol in a Transwell with 0.4 μm porous membranes, while DCs (1×10^5 cells/well) were seeded below the membranes of Transwell and cocultured for 24 h. Then the DCs were collected for flow cytometry analysis by the same method aforementioned.

To evaluate the vaccine effects of CpG@BSA-CaZol and CpG-MTX@BSA-CaZol on DC maturation, the K7M2 cells were cultured with these nanoagents in the upper chamber of the Transwell, while DCs (1×10^5 cells/well) were seeded below the membranes and cocultured for 24 h. To further verify the vaccine effect of these nanoagents *in vitro*, DCs (1×10^5 cells/well) were cultured with the supernatant which was collected from K7M2 treated with CpG@BSA-CaZol and CpG-MTX@BSA-CaZol for 24 h. Then the DCs were collected for flow cytometry analysis by the same method aforementioned.

Real-Time Imaging *In Vivo*. For *in vivo* fluorescence imaging, mice ($n = 3$) bearing K7M2 tumors were intravenously injected with BSA-CaZol, MTX@BSA-CaZol, and CpG-MTX@BSA-CaZol nanoparticles labeled with Cypate (200 μL, 1 mg mL^{-1}). The tumor-bearing mice were then imaged at various time points with IVIS Spectrum (PerkinElmer, USA). Then the major organs, left legs (containing tumor), and right legs were collected and imaged by IVIS Spectrum.

Antitumor Efficacy in K7M2 Mice Model. K7M2 tumor-bearing BALB/c mice were divided into five groups ($n = 8$ each group), i.e., (1) saline, (2) BSA-CaZol, (3) MTX@BSA-CaZol, (4) CpG@BSA-CaZol, and (5) CpG-MTX@BSA-CaZol. In each group, 200 μL of agent with the same BSA-CaZol equivalent concentration (5 mg mL^{-1}) was injected intravenously into each mouse twice on day 1 and day 4. The body weight of the mice and the volume of murine osteosarcoma were measured every second day.

For the short-term immunostimulatory experiment, 3 mice from each groups were sacrificed on the third day postinjection. The blood samples were collected from retro-orbital plexus of mice, and the TNF-α, IL-12, and IL-1β concentrations in serum were determined by ELISA. The tumors and lymph nodes were collected and sheared. Collagenase type IV (50 units/mL, Thermo Scientific) and DNase (20 units/mL, Roche) were added to digest extracellular components at 37 °C for 2 h. The cell suspensions of tumors were generated using a 70 μm strainer and centrifuged at 1500 rpm (4 °C, 5 min). After decanting the supernatant, cells were resuspended in 2 mL of PBS. The osteosarcoma tumor cells were divided into two portions: $CD4^+$ or $CD8^+$ T cells were gated on $CD45^+CD3^+$, DCs ($CD80^+CD86^+$) were gated on $CD11c^+F4/80^-$, respectively. The cells of lymph nodes for analyzing DC mutuation ($CD80^+CD86^+$) were gated on $CD11c^+F4/80^-$. All samples were also subjected to flow cytometry analysis. For ICD evaluation, tumor cells were stained with CRT antibody for cytometry analysis, and tumors were collected for HMGB-1 immunofluorescence analysis. All other mice organs were fixed in 10% formalin solution before the following assay.

For the long-term immunostimulatory experiment, the remaining mice from each group were sacrificed 3 weeks after the first injection. The following procedures for analyzing the blood were the same as those described above. The remaining tumor tissue and organs harvested were cut into slices of 10 μm and stained with H&E.

CD8 Depletion Experiment. K7M2 tumor-bearing BALB/c mice were intraperitoneally administered CD8 antibody (100 μg per mouse) to deplete CD8 T cells over 3 days. Then 200 μL of CpG-MTX@BSA-CaZol (5 mg mL^{-1}) was injected intravenously into each mouse on day 1 and day 4. The control mice ($n = 5$) were treated with saline. The volume of murine osteosarcoma was measured every second day.

Tumor Rechallenge Test. To study the immune memory effect, K7M2 cells (1×10^6) suspended in PBS were subcutaneously injected into the left flank of BALB/c mouse to establish the primary tumor. The primary tumor was intravenously administered CpG-MTX@BSA-CaZol (5 mg mL^{-1}) on day 1. Twenty-eight days later, K7M2 cells (1×10^6) suspended in PBS were subcutaneously injected into the left flank of BALB/c mice to establish the secondary K7M2 tumors. The age-matched naïve mice were used as the control. The volume of secondary tumors was measured every second day. The spleen of each mouse was collected for effector memory T cells (Tem) analysis ($CD3^+CD8^+$ $CD44^+CD62L^-$) on day 21.

To further verify the immune memory effect, the splenocytes from CpG-MTX@BSA-CaZol-treated mice were collected and cocultured with K7M2 cells. After 24 h, the splenocytes were stained with fluorescence-labeled CD3, CD8, IFN-γ, and Granzyme B antibodies and then analyzed by flow cytometry to detect the intracellular IFN-γ and Granzyme B production by CD8 T cells.

Antitumor Efficacy in 4T1 Mice Model. 4T1-Luc tumor-bearing BALB/c mice were divided into saline and CpG-MTX@BSA-CaZol groups ($n = 5$ each group). CpG-MTX@BSA-CaZol of 200 μL (5 mg mL^{-1}) was injected intravenously into each mouse twice on day 1. The tumor volume of murine breast cancer was measured with a vernier caliper every second day. The tumor-bearing mice were

https://doi.org/10.1021/acsnano.2c09685
ACS Nano 2023, 17, 6247−6260

imaged on days 1, 7, and 14 by IVIS Spectrum (PerkinElmer, USA). The lungs were collected on day 14 after the first injection.

ASSOCIATED CONTENT

Supporting Information

The Supporting Information is available free of charge at https://pubs.acs.org/doi/10.1021/acsnano.2c09685.

MTX of standard curve measured by absorbance (Figure S1); Cy5.5-labeled CpG of standard curve measured by absorbance (Figure S2); the surface charge of CpG-MTX@BSA-CaZol (Figure S3); agarose gel electrophoresis bands of free CpG and CpG-MTX@BSA-CaZol (Figure S4); 3T3 and K7M2 cell viability (Figure S5); maturation levels of DC coincubated with various treatments in Transwell system (Figure S6); maturation levels of DC coincubated with CpG@BSA-CaZol and CpG-MTX@BSA-CaZol alone (Figure S7); maturation levels of DC coincubated with supernatant of NPs-treated K7M2 cells (Figure S8); CRT and HMGB-1 expression levels in different treatments (Figure S9); CD86 and CD80 expression in TDLN under different treatments (Figure S10); ratio of CD8/CD4 in tumors (Figure S11); CD8 and CD4 immunofluorescence analysis of K7M2 tumor and spleen (Figure S12); fluorescence quantification of tumors and organs (Figure S13); blood biochemical analysis of CpG-MTX@BSA-CaZol treatment (Figure S14); tumor growth profiles and survival rate of MTX + Zol group (Figure S15); photographs of whole lungs collected from mice with different treatments (Figure S16); *in vivo* immune response of tumor with calcium phosphonate nano-agents at 21 days postinjection (Figure S17); photographs of whole spleens collected from mice with different treatments (Figure S18); flow cytometry plots of IFN-γ^+ $CD8^+$ and IFN-γ^+ $CD4^+$ T cells (Figure S19); immunofluorescence analysis of $CD11c^+$ DCs and TNF-α in the spleen (Figure S20); immunofluorescence analysis of $CD11c^+$ DCs and TNF-α in the tumor (Figure S21); ELISA analysis of IL-6 and IFN-γ, and H&E staining of tissues at 7 days postinjection (Figure S22); H&E staining tissues at 21 days postinjection (Figure S23); body weight in mice (Figure S24); CD8 depletion experiment (Figure S25); breast cancer treatment experiment (Figure S26); images of mice in the rechallenge experiment (Figure S27); intracellular IFN-γ and Granzyme B production by spleen $CD8^+$ T cells (Figure S28) (PDF)

AUTHOR INFORMATION

Corresponding Authors

Mingyuan Gao − *State Key Laboratory of Radiation Medicine and Protection, School of Radiation Medicine and Protection, Collaborative Innovation Center of Radiation Medicine of Jiangsu Higher Education Institutions, Soochow University, Suzhou 215123, China;* orcid.org/0000-0002-7360-3684; Email: gaomy@iccas.ac.cn

Yong Wang − *State Key Laboratory of Radiation Medicine and Protection, School of Radiation Medicine and Protection, Collaborative Innovation Center of Radiation Medicine of Jiangsu Higher Education Institutions, Soochow University, Suzhou 215123, China;* orcid.org/0000-0003-4061-7956; Email: yongwang@suda.edu.cn

Authors

Yangyun Wang − *State Key Laboratory of Radiation Medicine and Protection, School of Radiation Medicine and Protection, Collaborative Innovation Center of Radiation Medicine of Jiangsu Higher Education Institutions, Soochow University, Suzhou 215123, China;* orcid.org/0000-0002-2058-7553

Yanxian Wu − *State Key Laboratory of Radiation Medicine and Protection, School of Radiation Medicine and Protection, Collaborative Innovation Center of Radiation Medicine of Jiangsu Higher Education Institutions, Soochow University, Suzhou 215123, China*

Liubing Li − *Department of Orthopedic, The Second Affiliated Hospital of Soochow University, Suzhou 215004, China*

Chunjie Ma − *Department of Orthopedic, The Second Affiliated Hospital of Soochow University, Suzhou 215004, China*

Shaodian Zhang − *Department of Orthopedic, The Second Affiliated Hospital of Soochow University, Suzhou 215004, China*

Subin Lin − *Department of Orthopedic, The Second Affiliated Hospital of Soochow University, Suzhou 215004, China*

Leshuai W. Zhang − *State Key Laboratory of Radiation Medicine and Protection, School of Radiation Medicine and Protection, Collaborative Innovation Center of Radiation Medicine of Jiangsu Higher Education Institutions, Soochow University, Suzhou 215123, China;* orcid.org/0000-0002-6919-9180

Complete contact information is available at: https://pubs.acs.org/10.1021/acsnano.2c09685

Author Contributions

Y.Y. Wang, Y.X. Wu, and Y. Wang designed the study, performed experiments, analyzed and interpreted data, and wrote the manuscript. L.B. Li and C.J. Ma performed experiments. L.B. Li, S.D. Zhang, and Y.X. Wu interpreted the data. L.W. Zhang, Y. Wang, and M.Y. Gao revised the manuscript. Y.Y. Wang, Y.X. Wu, and L.B. Li contributed equally to this work.

Notes

The authors declare no competing financial interest.

ACKNOWLEDGMENTS

This work was supported by the National Natural Science Foundation of China (22122407, 12175162, 32171403, 12075164, 31971319, 12205214, 81972964), National Key Research Program of China (2018YFA0208800), Tang Scholar Program, the Scientific Research Program for Young Talents of China National Nuclear Corporation and A Priority Academic Program Development of Jiangsu Higher Education Institutions (PAPD).

REFERENCES

(1) Kansara, M.; Teng, M. W.; Smyth, M. J.; Thomas, D. M. Translational biology of osteosarcoma. *Nat. Rev. Cancer* **2014**, *14* (11), 722−735.

(2) Peinado, H.; Zhang, H.; Matei, I. R.; Costa-Silva, B.; Hoshino, A.; Rodrigues, G.; Psaila, B.; Kaplan, R. N.; Bromberg, J. F.; Kang, Y.; Bissell, M. J.; Cox, T. R.; Giaccia, A. J.; Erler, J. T.; Hiratsuka, S.; Ghajar, C. M.; Lyden, D. Pre-metastatic niches: organ-specific homes for metastases. *Nat. Rev. Cancer* **2017**, *17* (5), 302−317.

(3) de Nigris, F.; Ruosi, C.; Napoli, C. Clinical efficiency of epigenetic drugs therapy in bone malignancies. *Bone* **2021**, *143*, 115605−115605.
(4) Havel, J. J.; Chowell, D.; Chan, T. A. The evolving landscape of biomarkers for checkpoint inhibitor immunotherapy. *Nat. Rev. Cancer* **2019**, *19* (3), 133−150.
(5) Anandappa, A. J.; Wu, C. J.; Ott, P. A. Directing Traffic: How to Effectively Drive T Cells into Tumors. *Cancer Discovery* **2020**, *10* (2), 185−197.
(6) DeBerardinis, R. J. Tumor Microenvironment, Metabolism, and Immunotherapy. *N. Engl. J. Med.* **2020**, *382* (9), 869−871.
(7) Binnewies, M.; Roberts, E. W.; Kersten, K.; Chan, V.; Fearon, D. F.; Merad, M.; Coussens, L. M.; Gabrilovich, D. I.; Ostrand-Rosenberg, S.; Hedrick, C. C.; Vonderheide, R. H.; Pittet, M. J.; Jain, R. K.; Zou, W.; Howcroft, T. K.; Woodhouse, E. C.; Weinberg, R. A.; Krummel, M. F. Understanding the tumor immune microenvironment (TIME) for effective therapy. *Nat. Med.* **2018**, *24* (5), 541−550.
(8) Sullivan, R. J.; Weber, J. S. Immune-related toxicities of checkpoint inhibitors: mechanisms and mitigation strategies. *Nat. Rev. Drug Discovery* **2022**, *21* (7), 495−508.
(9) Melero, I.; Castanon, E.; Alvarez, M.; Champiat, S.; Marabelle, A. Intratumoural administration and tumour tissue targeting of cancer immunotherapies. *Nat. Rev. Clin. Oncol.* **2021**, *18* (9), 558−576.
(10) Saxena, M.; van der Burg, S. H.; Melief, C. J. M.; Bhardwaj, N. Therapeutic cancer vaccines. *Nat. Rev. Cancer* **2021**, *21* (6), 360−378.
(11) Kepp, O.; Marabelle, A.; Zitvogel, L.; Kroemer, G. Oncolysis without viruses - inducing systemic anticancer immune responses with local therapies. *Nat. Rev. Clin. Oncol.* **2020**, *17* (1), 49−64.
(12) Harari, A.; Graciotti, M.; Bassani-Sternberg, M.; Kandalaft, L. E. Antitumour dendritic cell vaccination in a priming and boosting approach. *Nat. Rev. Drug Discovery* **2020**, *19* (9), 635−652.
(13) Hammerich, L.; Marron, T. U.; Upadhyay, R.; Svensson-Arvelund, J.; Dhainaut, M.; Hussein, S.; Zhan, Y.; Ostrowski, D.; Yellin, M.; Marsh, H.; Salazar, A. M.; Rahman, A. H.; Brown, B. D.; Merad, M.; Brody, J. D. Systemic clinical tumor regressions and potentiation of PD1 blockade with in situ vaccination. *Nat. Med.* **2019**, *25* (5), 814−824.
(14) Wang, M.; Song, J.; Zhou, F.; Hoover, A. R.; Murray, C.; Zhou, B.; Wang, L.; Qu, J.; Chen, W. R. NIR-Triggered Phototherapy and Immunotherapy via an Antigen-Capturing Nanoplatform for Metastatic Cancer Treatment. *Adv. Sci.* **2019**, *6* (10), 1802157.
(15) Roy, D. G.; Geoffroy, K.; Marguerie, M.; Khan, S. T.; Martin, N. T.; Kmiecik, J.; Bobbala, D.; Aitken, A. S.; de Souza, C. T.; Stephenson, K. B.; Lichty, B. D.; Auer, R. C.; Stojdl, D. F.; Bell, J. C.; Bourgeois-Daigneault, M. C. Adjuvant oncolytic virotherapy for personalized anti-cancer vaccination. *Nat. Commun.* **2021**, *12* (1), 2626.
(16) Hu, Z.; Ott, P. A.; Wu, C. J. Towards personalized, tumour-specific, therapeutic vaccines for cancer. *Nat. Rev. Immunol.* **2018**, *18* (3), 168−182.
(17) Zheng, H.; Bae, Y.; Kasimir-Bauer, S.; Tang, R.; Chen, J.; Ren, G.; Yuan, M.; Esposito, M.; Li, W.; Wei, Y.; Shen, M.; Zhang, L.; Tupitsyn, N.; Pantel, K.; King, C.; Sun, J.; Moriguchi, J.; Jun, H. T.; Coxon, A.; Lee, B.; Kang, Y. Therapeutic Antibody Targeting Tumor- and Osteoblastic Niche-Derived Jagged1 Sensitizes Bone Metastasis to Chemotherapy. *Cancer Cell* **2017**, *32* (6), 731−747.
(18) Garassino, M. C.; Torri, V.; Colombo, M. P.; Sica, A. Choosing the Best Chemotherapy Agent to Boost Immune Checkpoint Inhibition Activity. *Cancer Res.* **2018**, *78* (20), 5729−5730.
(19) Cubas, R.; Moskalenko, M.; Cheung, J.; Yang, M.; McNamara, E.; Xiong, H.; Hoves, S.; Ries, C. H.; Kim, J.; Gould, S. Chemotherapy Combines Effectively with Anti-PD-L1 Treatment and Can Augment Antitumor Responses. *J. Immunol.* **2018**, *201* (8), 2273−2286.
(20) Liu, P.; Zhao, L.; Pol, J.; Levesque, S.; Petrazzuolo, A.; Pfirschke, C.; Engblom, C.; Rickelt, S.; Yamazaki, T.; Iribarren, K.; Senovilla, L.; Bezu, L.; Vacchelli, E.; Sica, V.; Melis, A.; Martin, T.; Xia, L.; Yang, H.; Li, Q.; Chen, J.; Durand, S.; Aprahamian, F.; Lefevre, D.; Broutin, S.; Paci, A.; Bongers, A.; Minard-Colin, V.; Tartour, E.; Zitvogel, L.; Apetoh, L.; Ma, Y.; Pittet, M. J.; Kepp, O.; Kroemer, G. Crizotinib-induced immunogenic cell death in non-small cell lung cancer. *Nat. Commun.* **2019**, *10* (1), 1486.
(21) Pelly, V. S.; Moeini, A.; Roelofsen, L. M.; Bonavita, E.; Bell, C. R.; Hutton, C.; Blanco-Gomez, A.; Banyard, A.; Bromley, C. P.; Flanagan, E.; Chiang, S.-C.; Jorgensen, C.; Schumacher, T. N.; Thommen, D. S.; Zelenay, S. Anti-inflammatory drugs remodel the tumor immune environment to enhance immune checkpoint blockade efficacy. *Cancer Discovery* **2021**, *11* (10), 2602−2619.
(22) Ringgaard, L.; Melander, F.; Eliasen, R.; Henriksen, J. R.; Jølck, R. I.; Engel, T. B.; Bak, M.; Fliedner, F. P.; Kristensen, K.; Elema, D. R.; Kjaer, A.; Hansen, A. E.; Andresen, T. L. Tumor repolarization by an advanced liposomal drug delivery system provides a potent new approach for chemo-immunotherapy. *Sci. Adv.* **2020**, *6* (36), No. eaba5628.
(23) Xiao, Z.; Su, Z.; Han, S.; Huang, J.; Lin, L.; Shuai, X. Dual pH-sensitive nanodrug blocks PD-1 immune checkpoint and uses T cells to deliver NF-κB inhibitor for antitumor immunotherapy. *Sci. Adv.* **2020**, *6* (6), No. eaay7785.
(24) Wang, Z.; Little, N.; Chen, J.; Lambesis, K. T.; Le, K. T.; Han, W.; Scott, A. J.; Lu, J. Immunogenic camptothesome nanovesicles comprising sphingomyelin-derived camptothecin bilayers for safe and synergistic cancer immunochemotherapy. *Nat. Nanotechnol.* **2021**, *16* (10), 1130−1140.
(25) Siemer, S.; Bauer, T. A.; Scholz, P.; Breder, C.; Fenaroli, F.; Harms, G.; Dietrich, D.; Dietrich, J.; Rosenauer, C.; Barz, M.; Becker, S.; Strieth, S.; Reinhardt, C.; Fauth, T.; Hagemann, J.; Stauber, R. H. Targeting Cancer Chemotherapy Resistance by Precision Medicine-Driven Nanoparticle-Formulated Cisplatin. *ACS Nano* **2021**, *15* (11), 18541−18556.
(26) Fu, L.-H.; Hu, Y.-R.; Qi, C.; He, T.; Jiang, S.; Jiang, C.; He, J.; Qu, J.; Lin, J.; Huang, P. Biodegradable Manganese-Doped Calcium Phosphate Nanotheranostics for Traceable Cascade Reaction-Enhanced Anti-Tumor Therapy. *ACS Nano* **2019**, *13* (12), 13985−13994.
(27) Dong, X.; Yang, A.; Bai, Y.; Kong, D.; Lv, F. Dual fluorescence imaging-guided programmed delivery of doxorubicin and CpG nanoparticles to modulate tumor microenvironment for effective chemo-immunotherapy. *Biomaterials* **2020**, *230*, 119659.
(28) Liu, S.; Jiang, Q.; Zhao, X.; Zhao, R.; Wang, Y.; Wang, Y.; Liu, J.; Shang, Y.; Zhao, S.; Wu, T.; Zhang, Y.; Nie, G.; Ding, B. A DNA nanodevice-based vaccine for cancer immunotherapy. *Nat. Mater.* **2021**, *20* (3), 421−430.
(29) Li, L.; Li, Y.; Yang, C. H.; Radford, D. C.; Wang, J.; Janát-Amsbury, M.; Kopeček, J.; Yang, J. Inhibition of Immunosuppressive Tumors by Polymer-Assisted Inductions of Immunogenic Cell Death and Multivalent PD-L1 Crosslinking. *Adv. Funct. Mater.* **2020**, *30* (12), 1908961.
(30) Wang, Q.; Lv, L.; Ling, Z.; Wang, Y.; Liu, Y.; Li, L.; Liu, G.; Shen, L.; Yan, J.; Wang, Y. Long-Circulating Iodinated Albumin-Gadolinium Nanoparticles as Enhanced Magnetic Resonance and Computed Tomography Imaging Probes for Osteosarcoma Visualization. *Anal. Chem.* **2015**, *87* (8), 4299−4304.
(31) Xu, Z.; Wang, Y.; Han, J.; Xu, Q.; Ren, J.; Xu, J.; Wang, Y.; Chai, Z. Noninvasive Multimodal Imaging of Osteosarcoma and Lymph Nodes Using a 99mTc-Labeled Biomineralization Nanoprobe. *Anal. Chem.* **2018**, *90* (7), 4529−4534.
(32) Wang, Y.; Sun, Z.; Chen, Z.; Wu, Y.; Gu, Y.; Lin, S.; Wang, Y. In Vivo Photoacoustic/Single-Photon Emission Computed Tomography Imaging for Dynamic Monitoring of Aggregation-Enhanced Photothermal Nanoagents. *Anal. Chem.* **2019**, *91* (3), 2128−2134.
(33) Yu, H.; Guo, H.; Zu, H.; Ding, H.; Lin, S.; Wang, Y.; Zhang, L. W.; Wang, Y. Therapeutic dendritic cell vaccines engineered with antigen-biomineralized Bi2S3 nanoparticles for personalized tumor radioimmunotherapy. *Aggregate* **2022**, *3*, e194.
(34) Qi, C.; Musetti, S.; Fu, L.-H.; Zhu, Y.-J.; Huang, L. Biomolecule-assisted green synthesis of nanostructured calcium phosphates and their biomedical applications. *Chem. Soc. Rev.* **2019**, *48* (10), 2698−2737.

https://doi.org/10.1021/acsnano.2c09685
ACS Nano 2023, 17, 6247−6260

(35) Wang, Y.; Lin, S.; Jiang, H.; Gu, Y.; Wu, Y.; Ma, J.; Ke, Y.; Zhang, L. W.; Wang, Y.; Gao, M. Visualizable Delivery of Nanodisc Antigen-Conjugated Adjuvant for Cancer Immunotherapy. *CCS Chem.* **2022**, *4* (4), 1238−1250.
(36) Wang, Y.; Wang, J.; Hao, H.; Cai, M.; Wang, S.; Ma, J.; Li, Y.; Mao, C.; Zhang, S. In Vitro and in Vivo Mechanism of Bone Tumor Inhibition by Selenium-Doped Bone Mineral Nanoparticles. *ACS Nano* **2016**, *10* (11), 9927−9937.
(37) Martínez-Vélez, N.; Xipell, E.; Vera, B.; Acanda de la Rocha, A.; Zalacain, M.; Marrodán, L.; Gonzalez-Huarriz, M.; Toledo, G.; Cascallo, M.; Alemany, R.; Patiño, A.; Alonso, M. M. The Oncolytic Adenovirus VCN-01 as Therapeutic Approach Against Pediatric Osteosarcoma. *Clin. Cancer Res.* **2016**, *22* (9), 2217−2225.
(38) Grippin, A. J.; Wummer, B.; Wildes, T.; Dyson, K.; Trivedi, V.; Yang, C.; Sebastian, M.; Mendez-Gomez, H. R.; Padala, S.; Grubb, M.; Fillingim, M.; Monsalve, A.; Sayour, E. J.; Dobson, J.; Mitchell, D. A. Dendritic Cell-Activating Magnetic Nanoparticles Enable Early Prediction of Antitumor Response with Magnetic Resonance Imaging. *ACS Nano* **2019**, *13* (12), 13884−13898.

https://doi.org/10.1021/acsnano.2c09685
ACS Nano 2023, 17, 6247−6260